Analysis of Reaction-Injection-Molded Polyurethanes by Near-Infrared Diffuse Reflectance Spectroscopy

CHARLES E. MILLER* and B. E. EICHINGER

Department of Chemistry, BG-10, University of Washington, Seattle, Washington 98195

SYNOPSIS

The ability of near-infrared (NIR) diffuse reflectance spectroscopy to characterize reaction-injection-molded (RIM) polyurethane elastomers is demonstrated. The advantage of NIR spectroscopy over other analytical methods is its ability to analyze samples without any preparation. In this work, the specific effects of composition, density, phase separation, and moisture content on the NIR spectra of the polymers are identified. In addition, the ability of NIR spectroscopy to make rapid assessments of physical properties, such as heat sag and flex modulus, is demonstrated. In order to perform these analyses, the multivariate statistical methods of principal components analysis (PCA) and partial least squares (PLS) are used.

INTRODUCTION

Reaction injection molding (RIM) is a common method of preparation for polyurethane products.[1] Polyurethane block copolymers produced by RIM are used predominantly for automotive applications.[2] The RIM process involves the mixing of two or more reactants and subsequent injection of the reactive mixture into a closed mold, where the curing reaction occurs. In the case of a reaction-injection-molded polyurethane product, the process involves the reaction between an isocyanate and a polyol blend. The polyol blend contains a polyol (a long-chain compound with reactive endgroups) and a chain extender (a low molecular weight compound with reactive endgroups). Subsequent reaction of these two parts results in a block copolymer with soft blocks (consisting primarily of the long-chain polyol) and hard blocks (consisting of the reaction product of the isocyanate and the chain extender). Specific information on polyurethane chemistry is covered in other references.[3-8]

A wide variation in end-use properties of RIM polyurethanes can be obtained by adjusting several parameters, such as the ratios of the three components in the reactants, the reaction temperature, and the catalyst concentration. Alterations in these parameters result in changes in chemical properties, such as composition, density, and phase separation, which greatly affect the physical properties of a RIM polyurethane material.[4-8] The performance of a RIM product is most commonly associated with its physical properties, such as modulus and impact resistance. As a result, any method that can be used to assess the performance of a RIM product must directly measure a physical property, or measure a chemical property that influences the physical property.

Thermal conductivity[9] and dynamic mechanical analysis[6,7,10,11] methods can be used to directly determine physical properties of RIM polyurethanes. Other analytical methods, such as FTIR,[7,8,10,12-16] differential scanning calorimetry,[4,6,10,17] and X-ray scattering[5-7,17] determine compositional and structural properties, which affect physical properties. Unfortunately, all of these methods require substantial sample preparation, and some of them are destructive. As a result, these methods cannot be used for rapid quality evaluation in a process environment.

In contrast, near-infrared (NIR) spectroscopy[18-20] can be used to rapidly and nondestructively analyze RIM polyurethanes. Unlike the methods mentioned

* To whom correspondence should be addressed; current address: Max-Planck-Institut fur Polymerforschung, Postfach 3148, D-6500 Mainz, Germany.

Journal of Applied Polymer Science, Vol. 42, 2169-2190 (1991)
 CCC 0021-8995/91/082169-22$04.00

above, NIR spectroscopy requires little or no sample preparation. NIR spectroscopy has been used extensively in the agricultural field as a method for rapid determination of moisture, protein and other constituents in bulk foods. Similarly, NIR spectroscopy can be used to determine constituents in bulk polymers.[21-25] Past studies have demonstrated the ability of NIR spectroscopy to determine chemical properties in polymers, such as composition,[21,23] phase separation,[24] crystallinity,[22] and microstructure.[25]

The major difficulty with NIR spectroscopy is the high overlap of bands from different functional groups. As a result, accurate NIR qualitative and quantitative analyses require the use of information from all available spectral frequencies. Multivariate statistical methods, such as principal components analysis (PCA)[26-28] and partial least squares (PLS),[26,29-31] have been used to successfully determine properties of materials from highly-convoluted NIR spectra.

In this work, near-infrared (NIR) spectroscopy is presented as a method to rapidly determine compositional and physical properties of block polyurethane copolymers produced by reaction injection molding (RIM). Principal components analysis (PCA) is used to identify variations in the NIR spectra of samples with differences in composition, density and phase separation. In addition, partial least squares (PLS) regression is used to correlate NIR spectra to various physical properties.

THEORY

Principal Components Analysis (PCA)[26-28]

In a typical NIR polymer analysis experiment, the data form a $m \times n$ response matrix $\mathbf{X}$, which contains the NIR spectra at n wavelengths for each of the m different polymer samples. Although n wavelengths are obtained for each sample, there might only exist f inherent variations in the spectra of the samples. As a result, the response matrix ($\mathbf{X}$) can be decomposed into a product of two matrices, according to the PCA model:

$$\mathbf{X} = \mathbf{T}\mathbf{P}^t + \mathbf{E} \qquad (1)$$

where $\mathbf{T}$ is an $m \times f$ matrix (called the PCA scores), $\mathbf{P}$ is an $n \times f$ matrix (called the PCA loadings), and $\mathbf{E}$ contains the spectral variation not explained by the PCA model. Given the response matrix $\mathbf{X}$, the PCA scores ($\mathbf{T}$) and loadings ($\mathbf{P}$) are determined by an iterative procedure such that the maximum variation in $\mathbf{X}$ is explained.

Each principal component in the PCA model has a corresponding loading spectrum and score vector. The kth principal component loading spectrum is obtained from the kth column of the $\mathbf{P}$ matrix, and the kth principal component scores are obtained from the kth column of the $\mathbf{T}$ matrix. The loading spectrum of a principal component indicates the NIR absorbance bands that are used to describe the principal component of variation in the spectra. The scores indicate the relationship between different samples, with respect to that principal component. As a result, the scores can be used to determine *whether* NIR spectroscopy distinguishes between samples with different properties, and the loadings spectra can be used to determine *how* NIR spectroscopy distinguishes between samples with different properties.

If there are known trends in several properties of the samples, there might exist an optimal rotation of the principal components such that the variations of each property are described by a single principal component. If such a rotation is accomplished, the effect of each property on the NIR spectroscopy of the samples is indicated by the loadings of one of the principal components. This procedure is very similar to graphical rotation, which has been used previously to improve the interpretability of mass spectrometry data.[32-37]

Partial Least Squares (PLS) Regression[26,29-31]

In contrast to the PCA method, the partial least squares (PLS) method constructs a model which relates the NIR spectrum of a sample to a specific property of the sample. In order to construct a PLS model, both the spectral responses and the values of the property of interest for all of the samples must be known. The PLS method involves two models: the spectrum model [eq. (1) above, where $\mathbf{X}$ contains the spectral responses for m calibration samples] and a property model, given by

$$\mathbf{y} = \mathbf{T}\mathbf{q} + \mathbf{f} \qquad (2)$$

where $\mathbf{y}$ is an $m \times 1$ vector containing the values of the property of interest for the m calibration samples, $\mathbf{q}$ is a $f \times 1$ vector, $\mathbf{f}$ is the residual for the property model, and $\mathbf{T}$ is a scores matrix. The PLS calibration algorithm determines $\mathbf{T}$, $\mathbf{P}$, and $\mathbf{q}$ such that the maximum variance in $\mathbf{X}$ that is correlated to $\mathbf{y}$ is explained. Because the PLS method has the extra task of explaining the variance in $\mathbf{y}$, the $\mathbf{T}$

and **P** matrices determined from the PLS method are usually different than the **T** and **P** matrices determined from the PCA method. The first PLS loading spectrum, which is obtained from the first column in the matrix **P** (determined by the PLS method), indicates the NIR spectral features that are positively and negatively correlated to the property of interest.

Cross-Validation

Cross-validation[26,27,31] is used to determine the optimal number of factors for both PCA and PLS analyses. Each cross-validation process involves the extraction of a subset of samples from the calibration samples, and the construction of PLS or PCA models with different numbers of factors from the remaining samples. The ability of each model to describe the spectra of the extracted samples (in the case of PCA) or the properties of the extracted samples (in the case of PLS) is then determined. The optimal number of factors is the number at which the addition of another factor to the model does not significantly improve the ability of the model to describe the spectra or properties of the extracted samples.

EXPERIMENTAL

Materials

Sample Set a

Samples in set **a** were prepared by the ICI Polyurethanes Group (Sterling Hgts., MI). The polyol formulations consisted of various mixtures of an ethylene–oxide-capped poly(propylene oxide) triol (with a molecular weight of approximately 6000) and diethyl toluene diamine (DETDA) chain extender. A small amount (approximately 0.24 mass %) of a typical polyurethane catalyst mixture was added to each polyol formulation. The isocyanate, prepared from the reaction of pure 4,4′-diphenylmethane diisocyanate (MDI) with a proprietary mixture of short-chain glycols, had a functionality of approximately 2 (23 mass % NCO). The ratio of polyol and chain extender concentrations was varied to produce RIM polymers with four different hard block percentages (approximately 55, 51, 46, and 42.5 mass %). After the samples were prepared, they were post-cured at 120°C for 1 h. The approximate chemical structure of the finished polyurethanes in sample set **a** is shown in Figure 1(A). It should be noted that side reactions during the RIM process and modification of the diisocyanate result in the presence of a small fraction of functional groups that are not shown in Figure 1(A).

A production-scale RIM machine (Cincinnati Milacron RIMM-90) was used to prepare the samples in set **a**. This machine produced 18 different polyurethane plaques 3 × 4 ft and 1/8 in. thick. The RIM samples were prepared with a mold temperature of 150°F (66°C) and a reactant temperature of 90°F (32°C). A heat sag sample (1 × 8 in.) and a flex modulus sample (1 × 3 in.) were cut from three different regions of each plaque: (1) the gate, corresponding to the part of the plaque closest to the injection point, (2) the middle, corresponding to the middle of the plaque, and (3) the end, corresponding to the part of the plaque farthest from the injection point. Flex modulus and heat sag samples from each of the three regions were cut from the center of the region, and were cut so that the long axis was parallel to the flow of material in the mold. Two replicate sets of 54 samples, one set for heat sag measurements and one set for flex modulus measurements, were obtained. The naming scheme for the samples used in this set is shown in Table I.

Sample Set b

The polyurethanes used in sample set **b** were prepared from the same polyol as the samples in set **a**. However, ethylene glycol was used as the chain extender, and the glycol-modified MDI was replaced by a proprietary prepolymer with average functionality of approximately 2.1. The approximate chemical structure of the polymers in sample set **b** is shown in Figure 1(B). In addition, a hard block model compound [Fig. 1(C)] was prepared from reaction of ethylene glycol (Aldrich) and phenyl isocyanate (Aldrich) in a dry nitrogen atmosphere. The model compound was rinsed five times with methanol and vacuum-dried for 24 h before use.

A research-scale RIM machine was used to prepare 1 × 1 ft and 1/8 in. thick polyurethane plaques. The mold temperature was 93°C, the mold time was 3 min, and the temperature of both reactants was 38°C for the preparation of all plaques. The percentage of ethylene glycol in the polyol reservoir (or the formulation) was varied between four different levels (9.1, 12.4, 16.4, and 20 mass %); these formulations resulted in the production of polyurethanes with hard block percentages of approximately 40, 47.5, 55, and 60 mass %, respectively. The index, which refers to the relative amounts of material in the isocyanate and polyol reservoirs that are mixed during an injection, was also varied between four

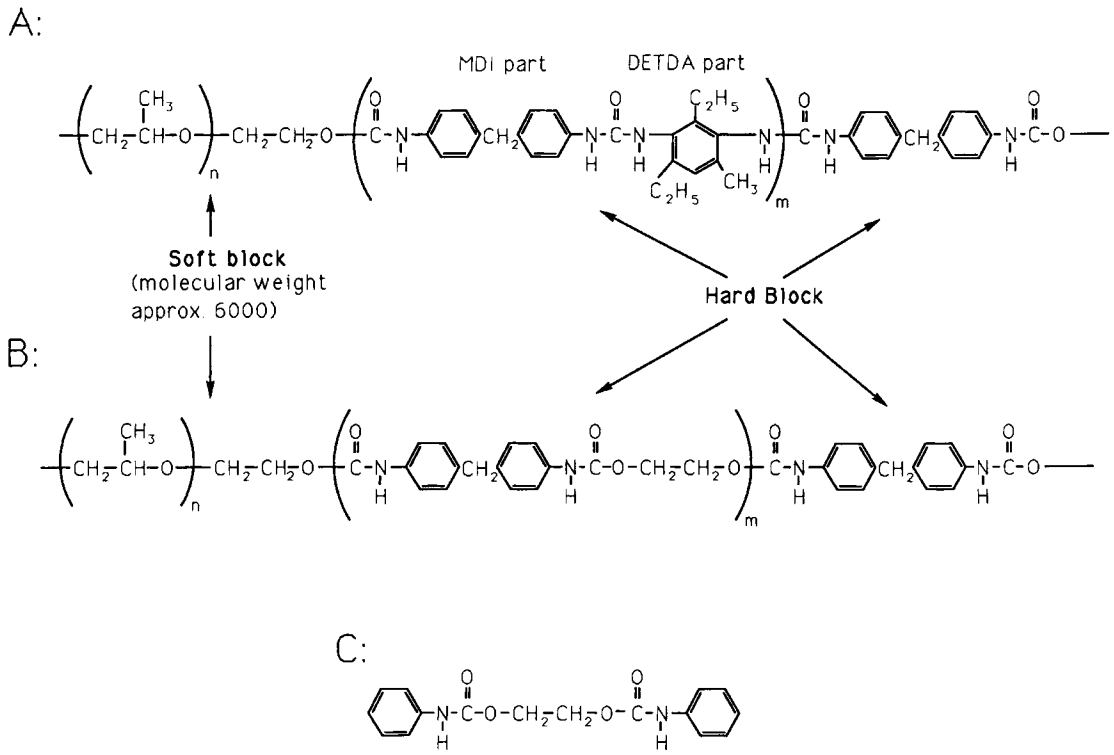

Figure 1 Chemical structures of RIM polyurethanes in sample set **a** (A) and sample set **b** (B), and the chemical structure of the hard block model compound for the sample set **b** samples (C). For Figure 1(A), the structure does not indicate modification of the isocyanate.

different levels (101, 104, 106, and 109). An index of 100 corresponds to the mixing ratio for perfect reaction stoichiometry, and an increase in the index corresponds to an increase in the excess isocyanate in the reaction. Two plaques were prepared from each possible combination of formulation and index. In each case, one of the plaques was post-cured at 120°C for 1 h and the other was not. The experimental design and naming scheme for the 32 plaques are shown in Table I. Three 1 × 3 in. samples for flex modulus testing and three 1 × 8 in. samples for heat sag testing were cut from each of the 32 original plaques. Some of the plaques, which had visible nonhomogeneities (presumably from incomplete mixing during the reaction), yielded fewer physical test samples. A total of 90 1 × 3 in. flex modulus samples and 83 1 × 8 in. heat sag samples were prepared.

NIR Spectroscopy and Physical Testing

NIR diffuse reflectance spectra were obtained with a Technicon InfraAlyzer 500C grating instrument. The nominal resolution of the instrument was 10 nm, and the wavelength accuracy was ±1 nm. Duplicate NIR diffuse reflectance spectra of each physical testing sample were obtained, using the sampling arrangement shown in Figure 2. The spectrometer used in this work utilized an integrating sphere for efficient collection and detection of diffusely reflected light. Duplicate NIR sampling was done near the center of each sample, and a diffusely reflecting ceramic background was used for all measurements. All samples were cleaned with hexane before analysis. An NIR pseudo-absorbance value, which is equal to $\log(1/R)$ (where R is the intensity of light reflected by the sample), was obtained at every 8 nm from 1100 to 2236 nm for the flex modulus samples in set **a**, at every 4 nm from 1101 to 2249 nm for the heat sag samples in set **a**, and at every 8 nm from 1102 to 2200 nm for all samples in set **b**. The averages of the replicate spectra for each sample were used for analysis. Multiplicative scatter correction (MSC)[38,39] was then used to reduce baseline offset and multiplicative scatter effects in the spectra. For both sample sets **a** and **b**, the flex modulus samples were used for PCA and PLS studies, and the heat sag samples were used only for PLS studies.

Table I Experimental Design and Naming Scheme for Samples in Set a and Set b

Sample Set **a**

First character: composition group
A: approximately 55 mass % hard block
B: approximately 51 mass % hard block
C: approximately 46 mass % hard block
D: approximately 42.5 mass % hard block
Second character: sample number within composition group
1–3 for group A
1–5 for groups B, C, and D
Third character: location of sample in RIM plaque:
G: gate; from one-third of plaque closest to injection point
M: middle; from middle one-third of plaque
E: end; from one-third of plaque farthest from injection point

Sample Set **b**

	Percentage of Ethylene Glycol in Polyol Reservoir (Approximate Hard Block Percentage[a])			
Index[a]	9.1 (40)	12.4 (47.5)	16.4 (55)	20.0 (60)
101	D1N[b]	C1N	B1N	A1N
	D1Y[c]	C1Y	B1Y	A1Y
104	D2N	C2N	B2N	A2N
	D2Y	C2Y	B2Y	A2Y
106	D3N	C3N	B3N	A3N
	D3Y	C3Y	B3Y	A3Y
109	D4N	C4N	B4N	A4N
	D4Y	C4Y	B4Y	A4Y

[a] Hard block percentage is also affected by index.
[b] N = not post-cured sample.
[c] Y = post-cured sample (120°C for 1 h).

NIR spectra of the pure polyol, pure diisocyanate, and a 1% (w/v) solution of the hard block model compound in tetrahydrofuran (THF) (Baker) were obtained with the samples in a 1 mm path length glass cuvette. In each case, the spectrum was collected in "transflectance" mode (with the cuvette placed in front of a diffusely reflecting ceramic background). The spectrum of the model compound in THF was obtained from a weighted subtraction of the spectrum of pure THF from the solution spectrum. The diffuse reflectance spectrum of the bulk hard block model compound was obtained with a sampling cell that was developed for small samples.[40]

After the samples were analyzed by NIR spectroscopy, they were tested for flex modulus and heat sag. These tests were performed with a Universal testing machine (Instron). The flex modulus was determined using a 2-in. span of the sample and a 0.55 in./min crosshead speed (ASTM Method D-790-86).[41] Single flex modulus measurements at 23, 38, and 70°C were done for each 1 × 3 in. sample in sample set **a**, and a single flex modulus measurement at 23°C was done for each 1 × 3 in. sample in sample set **b**. The heat sag measurement of each 1 × 8 in. sample involved horizontal placement of the sample with a 6-in. overhang, and subsequent observation of the sag of the overhang as the sample was exposed to 120°C for 1 h (ASTM Method D-3769-85).[42] A single heat sag measurement was made for each 1 × 8 in. sample in both sample sets.

It should be noted that after preparation, the samples in set **a** were stored for 16 months before NIR analysis and 17 months before physical testing. For the set **b** samples, NIR analysis and physical testing were performed only 2 months after preparation of the samples.

Data Analysis

Principal components analysis of the NIR spectra of the flex modulus samples was done with software provided by the Center For Process Analytical Chemistry (CPAC, University of Washington, Seattle WA).[43] Two analyses were done, one each for the two sample sets. All spectra were mean-centered (i.e., the mean spectral intensity of the samples in the data set is subtracted from the absorbance of each sample, for every wavelength point in the spectrum) before PCA analyses. Cross-validation was used to determine the optimal number of principal components. Graphical rotation[32–37] of the first two

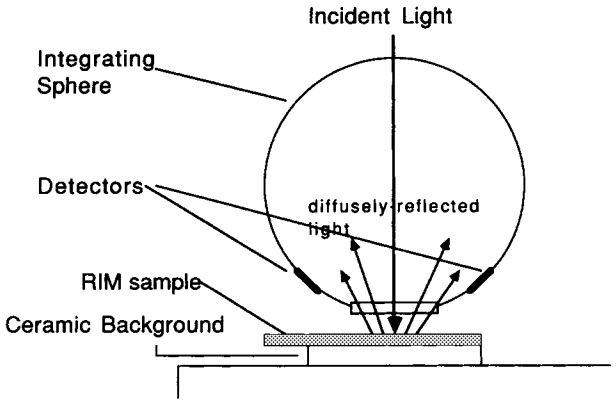

Figure 2 Sampling arrangement for near-infrared diffuse reflectance spectroscopy of RIM polyurethanes.

principal components obtained from the sample set **a** spectra was performed in a LOTUS-123 spreadsheet.

PLS correlations of NIR spectra to physical properties were done with software provided by CPAC.[44] For each PLS analysis, the samples were split into calibration and prediction sets. Samples in the calibration set were used to construct PLS models, and samples in the prediction set were used to test the validity of the PLS models. The method of cross-validation was used to determine the optimal number of spectral factors for all calibrations. Four different properties were calibrated to NIR spectra of the **a** samples (flex moduli at 23, 38, and 70°C and heat sag) and two properties were calibrated to NIR spectra of the **b** samples (flex modulus at 23°C and heat sag). All spectra were mean-centered before PLS modeling.

Two error statistics were obtained for each PLS calibration: the standard error of estimate (SEE) and the standard error of prediction (SEP). The SEE value is a measure of calibration error:

$$\mathrm{SEE} = \left[\frac{\sum_{i=1}^{\mathrm{NC}} (\hat{C}_{i,c} - C_{i,c})^2}{(\mathrm{NC} - 1)} \right]^{1/2} \quad (3)$$

where $\hat{C}_{i,c}$ is the property of calibration sample i that is estimated from the calibration model, $C_{i,c}$ is the known property of calibration sample i, and NC is the number of calibration samples. The SEP is a measure of prediction error:

$$\mathrm{SEP} = \left[\frac{\sum_{i=1}^{\mathrm{NP}} (\hat{C}_{i,p} - C_{i,p})^2}{\mathrm{NP}} \right]^{1/2} \quad (4)$$

where $\hat{C}_{i,p}$ is the property of prediction sample i that is predicted from the calibration model, $C_{i,p}$ is the known property of prediction sample i, and NP is the number of prediction samples. Relative error was calculated as the standard error divided by the range of property values used in the analysis.

Moisture Study

Sample A2E (in sample set **a**) was dried by heating in a dry nitrogen-purged oven at 120°C for 1.5 h. The sample was then exposed to the atmosphere at room temperature for 20 additional hours. The mass of the sample (obtained from a Mettler balance) and its NIR spectrum were obtained before drying, after drying, and after exposure to the atmosphere. After the drying step, the sample was allowed to cool at room temperature for 20 min before weighing and NIR sampling.

RESULTS AND DISCUSSION

NIR Band Assignments

Figure 3 shows the NIR spectrum of polyurethane sample B4Y in sample set **b** (A) and the spectrum of the modified MDI (B) and polyol (C) that were used to prepare the polymers in both samples sets. The bands in the polymer spectrum (A) at 1184, 1220, 1416, 1688, and 1732 nm, which are also observed in the spectrum of the polyol (C), correspond to aliphatic CH groups in the soft block of the polymers.[23] Bands at 1146, 1648, and 2162 nm in the polymer spectrum, which are at approximately the same positions as bands in the spectrum of modified MDI (B), correspond to aromatic CH groups in the MDI part of the hard block of the polymer.[23] The band of 1764 nm in the polymer spectrum, which is also in the spectrum of the modified MDI, probably corresponds to the bridging methylene group of MDI [see Figs. 1(A) and (B)].[23] The band at 1874 nm in the spectrum of the modified MDI (B) is from the isocyanate group. Several bands in the polymer spectrum that are not observed in the polyol or diisocyanate spectrum (1496, 1920, and 2048 nm) correspond to urethane groups in the polymer. The 1496 and 2048 nm bands are from NH vibrations in the urethane group. The absorbance at 1920 nm is probably the result of overlapping bands from the urethane carbonyl group and from water in the polymer.[24]

The NIR spectra of the samples in sample set **a** are very similar to the spectra of the samples in sample set **b**. As a result, the above band assignments for functional groups are reasonably accurate for samples in both sample sets. The only major difference between the samples in set **a** and set **b** is that the set **a** samples [Fig. 1(A)] have urea and urethane groups in the hard block, and the set **b** samples [Fig. 1(B)] have only urethane groups in the hard block. This difference causes the spectra of the samples in the two different sets in the NH and carbonyl regions (1450–1600 nm and 1900–2100 nm) to differ considerably.

Phase separation in polyurethane block copolymers involves hydrogen bonding between hard blocks in the polymer.[15,16] The effect of phase separation in the polyurethanes in sample set **b** is ap-

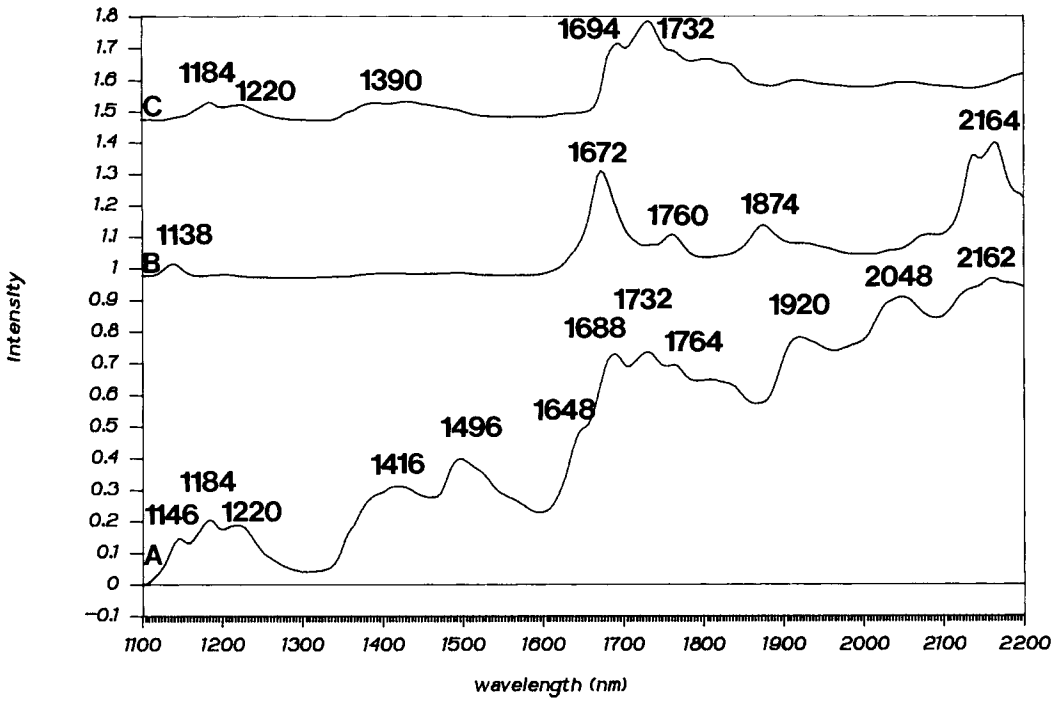

Figure 3 Near-infrared diffuse reflectance spectrum of polyurethane sample B4Y (in sample set **b**) (A), and near-infrared transflectance spectra of the modified 4,4'-diphenylmethane diisocyanate (B) and polyol (C), which were used to prepare the polymers in set **b**.

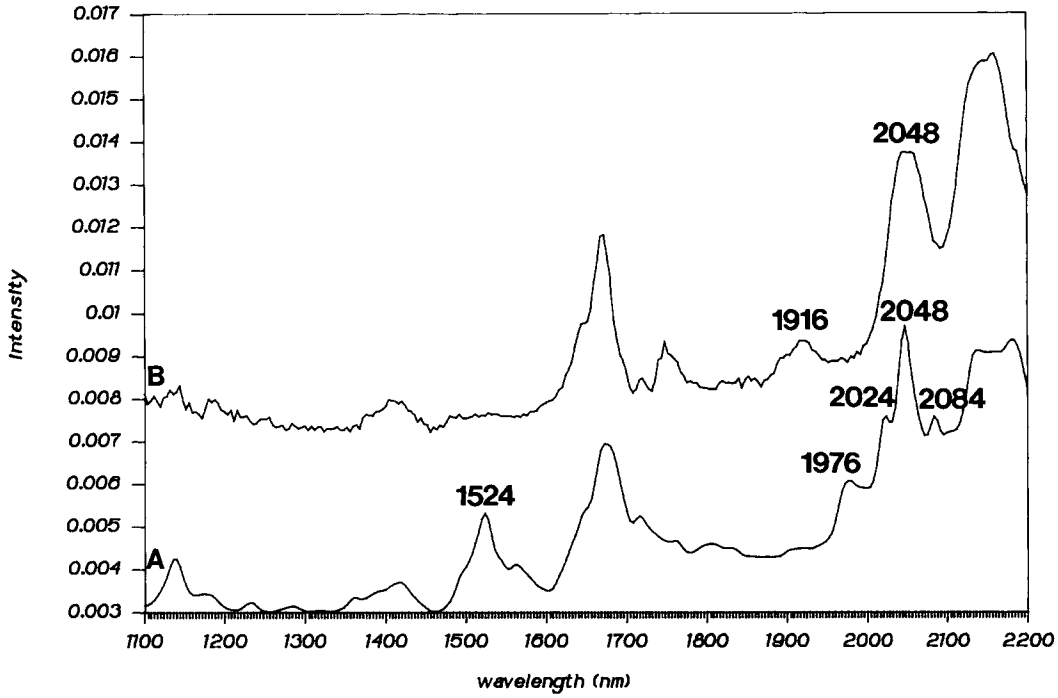

Figure 4 NIR diffuse reflectance spectrum of the bulk hard block model compound for the sample set **b** samples (A), and the transflectance spectrum of the hard block model compound in THF solution (B). The calculation of spectrum B is described in the text.

proximated by comparison of the spectrum of the bulk hard block model compound [Fig. 4(A)] and the model compound in dilute THF solution [Fig. 4(B)]. In the bulk compound, which is a crystalline material, discrete hydrogen bonds between urethane NH and carbonyl groups are present. In solution, most urethane NH groups are hydrogen-bonded to solvent molecules, and the urethane carbonyl groups are free from hydrogen bonding. Major differences in these spectra are observed in the regions of carbonyl and NH absorptions (1900–2100 nm and 1500–1600 nm). The 1976 nm band in the bulk model compound spectrum (A) corresponds to a carbonyl group that is hydrogen-bonded to NH groups in the bulk model compound. The 1916 nm band in the solution spectrum (B) corresponds to the free urethane carbonyl group. Three separate combination bands in the NH region (2024, 2048, and 2084 nm) are observed in the spectrum of the bulk model compound (A). It is unlikely that these three bands correspond to three hydrogen-bonded states of the NH group in the bulk model compound, because earlier studies[45] indicate that only one type of hydrogen bond is formed in the crystal structure of a similar model compound. Therefore, these three bands might arise from the combinations of the NH stretching mode with three different vibrational modes in the crystal. The spectrum of the model compound in solution has only a single broad NH combination band at 2048 nm. This band results from a continuous distribution of hydrogen-bonded states of the urethane NH groups in solution.

A strong band at 1524 nm in the spectrum of the bulk model compound, which is not present in the solution spectrum, is a first overtone band of the NH group in the crystalline bulk model compound. The reason for the absence of the 1524 nm band in the solution spectrum is uncertain. However, these results indicate that this band corresponds to an aggregated state of hard segments in the sample set **b** polymers.

Unfortunately, the NIR spectral effects of phase separation of the samples in set **a** are different than the effects of phase separation observed in this study, because the hard blocks of the polymer are different for the two sample sets [see Figs. 1(A) and (B)]. Earlier phase separation studies,[24] which used polyurethanes with urea groups in the hard blocks (like the samples in sample set **a**), indicate that phase separation in this polymer system is accompanied by increased hydrogen bonding of urea carbonyl groups (which involves a decrease is absorbance at 2034 nm) and decreased hydrogen bonding of urethane carbonyl groups (which involves an increase in absorbance at 1918 nm).

Principal Components Analysis Results

Sample Set a

PCA cross-validation results indicate that three spectral factors are necessary to explain the variations in the NIR spectra of the RIM polyurethanes in sample set **a**. In addition, the first two principal components obtained from the original PCA procedure were rotated −38°, in order to provide more interpretable results. The first, second, and third principal components in the rotated PCA model explain 49.5, 44.4, and 3.3% of the spectral variation, respectively.

Figure 5 shows a plot of the principal component 1 versus the principal component 2 scores for the rotated PCA model. Note that the variation between the samples with different composition (denoted by the first character of the sample name) is described by the second principal component, and the variation between the samples obtained from different parts of the original RIM plaque is described by the first principal component.

Several important properties of RIM polymers are known to vary between different spatial regions of a plaque.[46] One of these properties, the polymer density, is related to the concentration of nitrogen voids in the polymer. The process of nucleation, which occurs during the RIM process, involves the liberation of nitrogen that was formerly dissolved in the reactants. As the polymer cures, the liberated nitrogen gas becomes trapped in the polymer. The voids produced by this process enhance the diffuse reflectance and decrease the density of the product. The density of a RIM sample is a very important property, because it strongly affects the physical properties of the sample. In this study, it is observed that the concentration of voids in a polyurethane plaque increases (and thus the density decreases) as one moves from the injection end of the plaque (the gate) to the end of the plaque.[1]

The first principal component loading spectrum [shown in Fig. 6(A)], which explains the spectral variation that corresponds to differences in the gate, middle, and end portions of the same RIM piece, is very interesting. Comparison of this loading spectrum with the spectrum of a typical polyurethane used in this analysis [Fig. 3(A)] indicates that the loading spectrum has negative bands of the polymer spectrum at short wavelengths (1100–1600 nm) and

positive bands of the polymer spectrum at longer wavelengths (1600–2250 nm). In summary, the first principal component loading indicates an enhancement of longer wavelength diffuse reflectance intensities relative to shorter wavelength intensities. The intensities in the diffuse reflectance spectra in this work are expressed in pseudo-absorbance units which are calculated as $\log(1/R)$, where R is the intensity of collected diffusely reflected light (if no specular reflectance is present). An increase in measured pseudo-absorbance occurs both from absorption of incident light by the sample and from loss of diffusely-reflected light. In several illustrations, Birth and Hecht[47] indicate that increasing scattering ability of a sample causes more diffuse reflectance at wider angles from the incident light (refer to Fig. 2). In this work, diffusely reflected light is collected within a confined range of angles. Therefore, an increase in scattering ability of the sample would be expected to cause an increase in undetected diffusely reflected light, and thus an increase in measured pseudo-absorbance for a sample.

It is possible that the scattering ability (and thus the loss of diffusely reflected light) is not constant for all wavelengths. Because the voids in the RIM polymers are much larger than the wavelength of light used in the spectral studies, the scattering ability of a RIM sample depends on the regular reflection of light at each void/polymer interface in the material, which is described by one of the Fresnel equations[47,48]:

$$R_{\text{void/polymer}} = \frac{(n_2 - n_1)^2 + n_2^2\kappa^2}{(n_2 + n_1)^2 + n_2^2\kappa^2} \qquad (5)$$

where $R_{\text{void/polymer}}$ is the reflectance at a void/polymer interface, n_1 is the refractive index of the void, n_2 is the refractive index of the polymer, and κ is the absorption coefficient of the polymer. It is well known that shorter-wavelength NIR bands have lower absorptivities than longer-wavelength NIR bands.[19] Equation (5) indicates that significantly more diffuse reflectance is obtained for the stronger-absorbing wavelengths (the longer wavelengths) than for the weaker-absorbing wavelengths (the shorter wavelengths) for samples with many void/polymer interfaces. Therefore, an increase in scattering ability (density of voids) of an RIM sample is expected to enhance the diffuse reflectance intensities of longer wavelengths greater than for shorter wavelengths. This mechanism might explain the correlation of the first principal component to sample density.

Figure 5(B) indicates that the second principal component describes the variation between the spectra of samples in different composition groups. The second principal component loading spectrum [Fig. 6(B)] supports this conclusion. The positive peaks at 1140, 1648, 2124, and 2156 nm correspond to aromatic CH bands in the hard block of the polymer.[23] The positive NH band at 1496 nm and the carbonyl band at 1984 nm also indicate a positive correlation to hard block percentage. The most prominent negative peaks, at 1228 and 1732 nm, correspond to aliphatic CH groups,[21,23] which are a major component of the soft block of the polymers. Therefore, the loading spectrum indicates that the second principal component is positively correlated to the hard block percentage (or the composition) of the samples.

A plot of the third principal component scores versus the first principal component scores (Fig. 7) indicates that the third principal component describes a variation between the two groups of polymers with the highest hard block percentages (groups A and B). The third principal component loading spectrum is shown in Figure 8. Positive aliphatic CH peaks at 1188, 1228, 1704, and 1740 nm and negative aromatic CH peaks at 1644 and 2152 nm indicate a negative correlation of this component with hard block percentage.

Additional features in the third principal component loading spectrum (Fig. 8) at 1484, 1548, 1588, 1936, and 2076 nm correspond to carbonyl and NH groups.[19] First overtone NH stretching bands at 1484, 1548, and 1588 nm are assigned on the basis of earlier assignments of IR bands in similar model polyurethanes.[15,16] The sharp negative band at 1484 nm is the first overtone band of the free NH group. The sharpness of this band is indicative of non-hydrogen-bonded species.[49–52] The positive bands at 1548 and 1588 nm correspond to hydrogen-bonded NH groups. The positive band at 2076 nm is probably a combination amide II and NH stretching band. The negative peak at 1936 nm might correspond to a free urethane carbonyl group, but the overlap of water absorbances makes interpretation of this feature very tentative.[24]

The loading spectrum indicates that the third principal component is correlated to a change in the hydrogen-bonding states of NH groups in the polymers. Although this effect probably corresponds to a change of phase separation in the polymers, it is not certain whether is it positively or negatively correlated to phase separation. Detailed NIR investigations of phase separation of these polymers, or

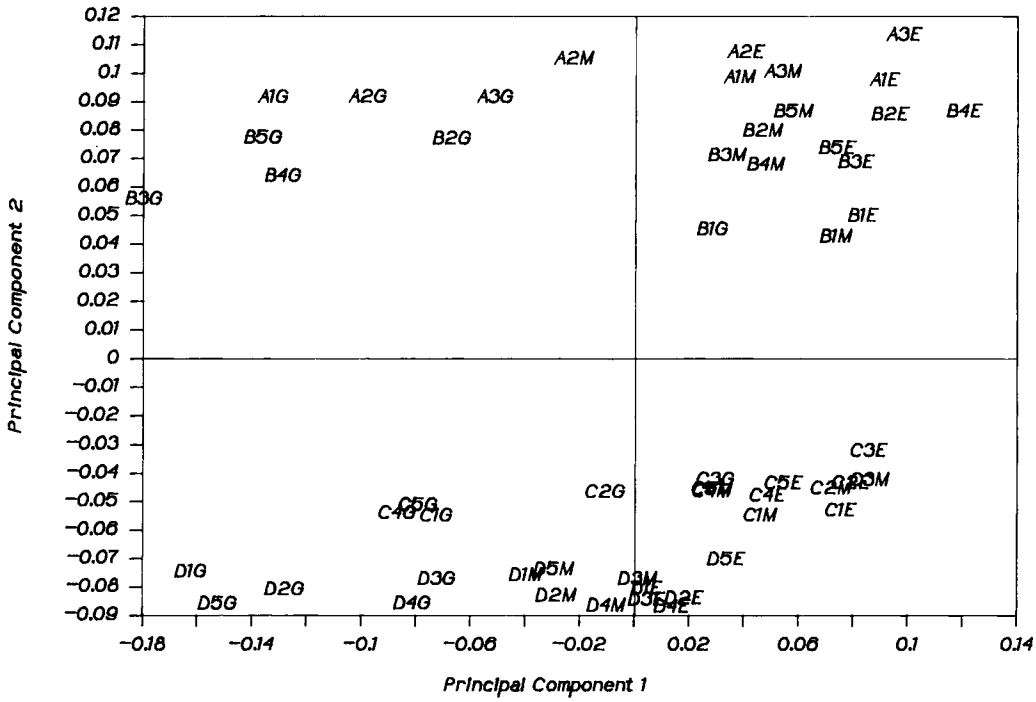

Figure 5 Plot of the second versus the first principal component scores for rotated PCA model, obtained from principal components analysis of the NIR spectra of the RIM polyurethanes in sample set **a**. Sample names are described in Table I.

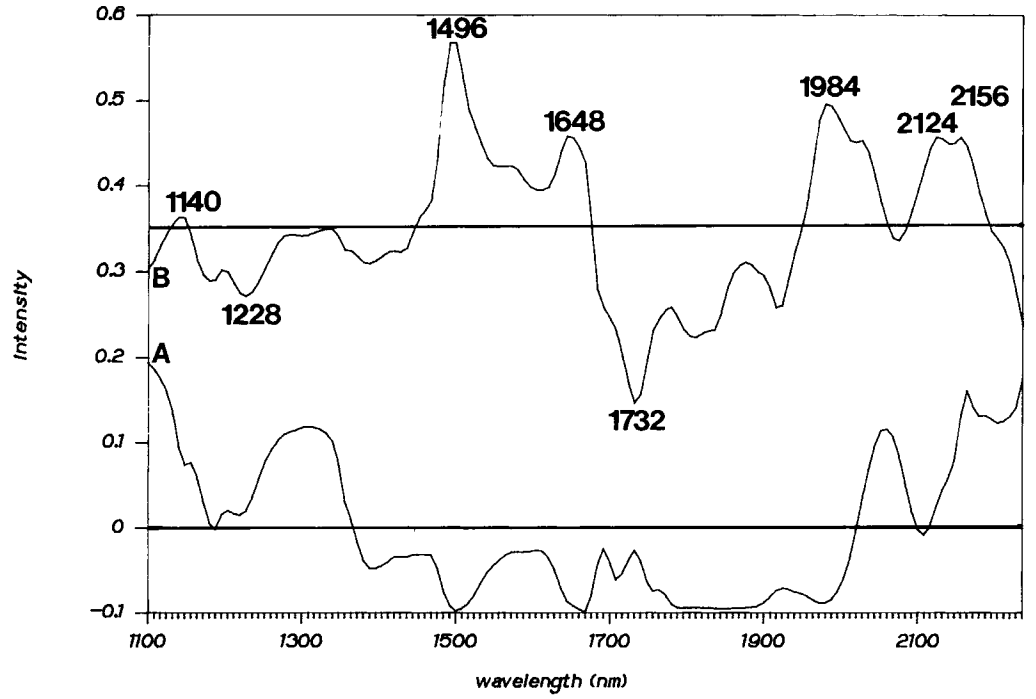

Figure 6 The loadings spectra for principal component 1 (A) and principal component 2 (B), obtained from principal components analysis of the NIR spectra of the RIM polyurethanes in sample set **a**.

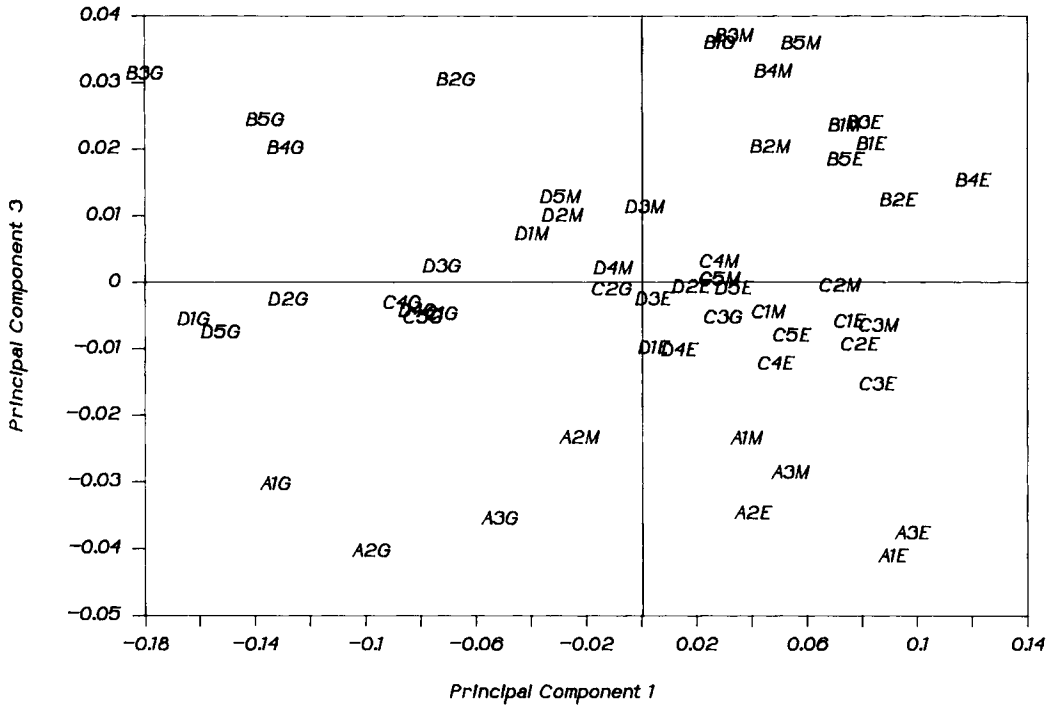

Figure 7 Plot of the third versus the first principal component scores, obtained from principal components analysis of the NIR spectra of the RIM polyurethanes in sample set **a**.

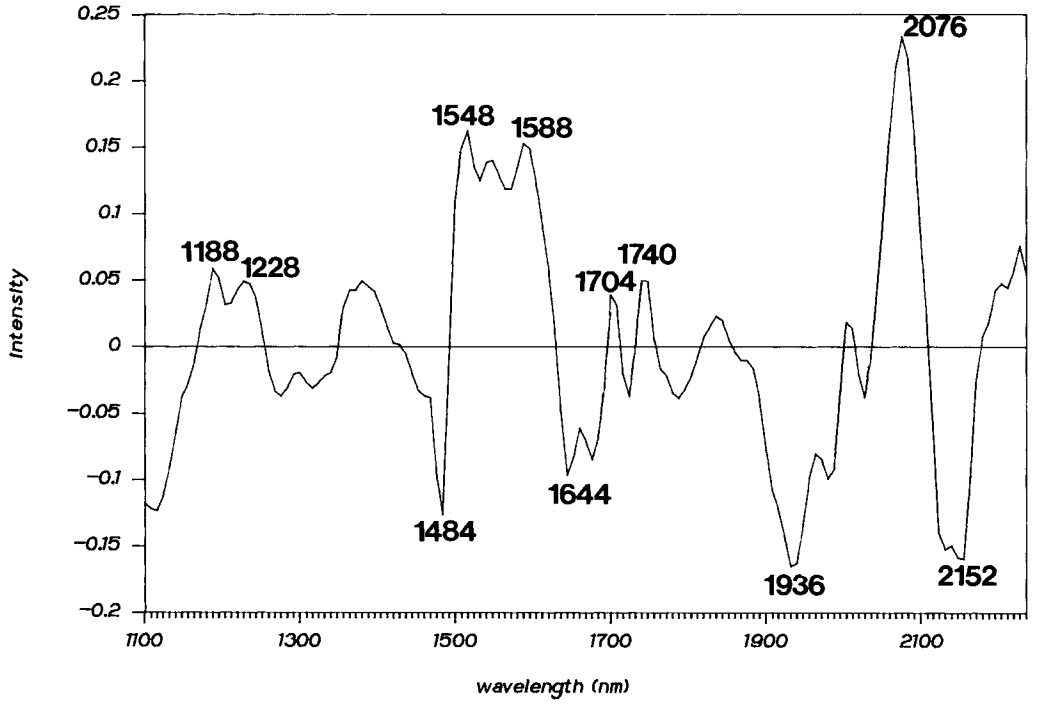

Figure 8 The third principal component loading spectrum, obtained from principal components analysis of the NIR spectra of the RIM polyurethanes in sample set **a**.

analyses of an appropriate hard block model compound for these polymers, are necessary to determine whether this principal component indicates an increase or decrease of phase separation. However, this result suggests that NIR spectroscopy can be used to monitor the effect of phase separation on the NH groups in the polymer. Earlier FT-IR investigations[15,16] could not fully characterize the effect of phase separation on NH groups, because the fundamental free NH stretching band is very weak relative to fundamental hydrogen-bonded NH bands. In contrast, NIR overtone stretching bands for hydrogen-bonded and non-hydrogen-bonded NH groups are of comparable intensity.

The PCA results indicate that the samples in composition group A have a different degree of phase separation than the samples in composition group B. It is known that phase separation in RIM polyurethanes depends on several reaction parameters, such as catalyst concentration and reaction temperature.[6-8] It is quite possible that the samples in the two composition groups were prepared under slightly different reaction conditions. Unfortunately, no significant differences in the preparation of these samples are known, and we therefore cannot confirm this assertion.

Sample Set b

Cross-validation result indicate that three principal components describe the variation in the NIR spectra of the flex modulus in set **b**. The first principal component explains 71.7% of the spectral variation, the second principal component explains 19.7%, and the third principal component explains 3.9%. It should be noted that no rotation of the principal components was necessary to improve the interpretation of the results.

The loadings spectra for the three principal components, shown in Figure 9, indicate the properties that are explained by each principal component. The first principal component loading spectrum (A) has positive aromatic CH bands at 1142 and 1654 nm, positive urethane NH bands at 1494 and 2094 nm, a positive urethane carbonyl band at 1998 nm, and a negative aliphatic CH band at 1734 nm. These bands indicate that the first principal component is positively correlated to the hard block percentage of the polymer.

The second principal component loading spectrum [Fig. 9(B)] has a negative aliphatic CH peak at 1182 nm, a negative NH peak at 1494 nm, a positive NH peak at 2054 nm, and a positive aromatic

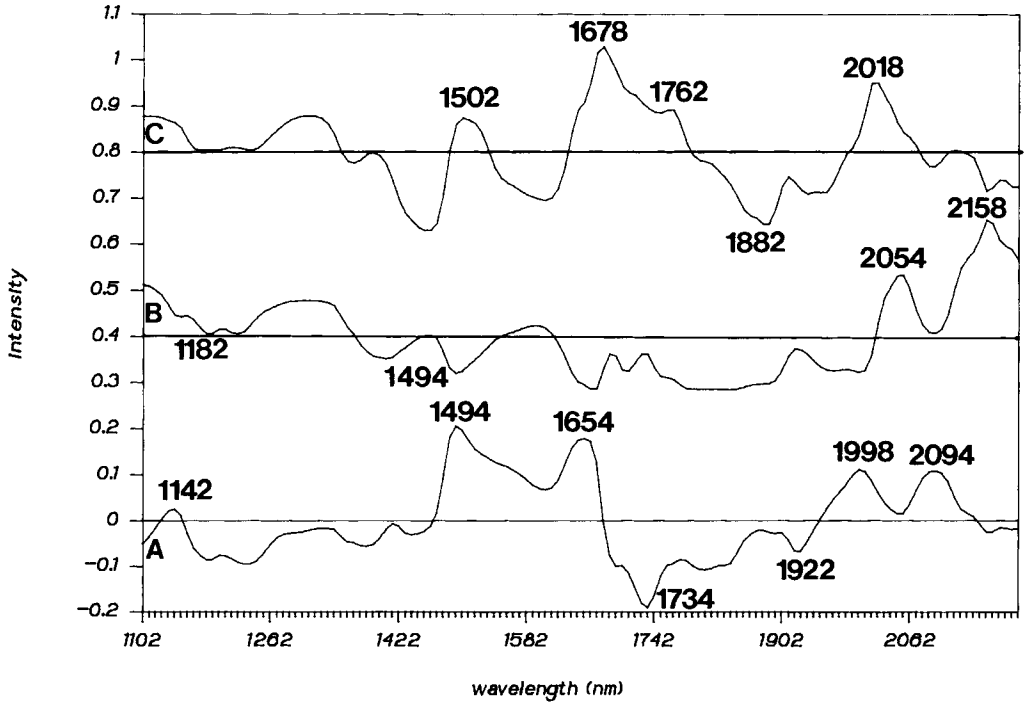

Figure 9 Principal component loadings spectra for the first (A), second (B), and third (C) principal components, obtained from principle components analysis of the NIR spectra of the polyurethane samples in set **b**.

CH peak at 2158 nm. This loading spectrum is almost identical to the first loading spectrum obtained from principal components analysis of the samples in set **a** [Fig. 6(A)]. In the previous section, it was determined that a loading spectrum of this type indicates a negative correlation to density. Therefore, it can be concluded that the second principal component in this analysis is negatively correlated to density.

The principal component correlated to density in this analysis explains a lower percentage of the spectral variation (19.7%) than the principal component correlated to density in the analysis of samples in set **a** (49.5%). Because the variations from other properties (such as composition) are expected to be nearly equal for the samples in set **a** and set **b**, it can be concluded that the densities of the samples in set **b** vary less than the densities of the samples in set **a**. This result suggests that the density gradients across individual RIM plaques prepared from the large mold (3 × 4 ft, as in the sample set **a** study) were larger than the density gradients across individual plaques prepared from the smaller mold (1 × 1 ft, as in this study).

The 2-dimensional scores plot for the first and second principal components is shown in Figure 10. The four distinct clusters of samples in the scores plot correspond to the four composition classes of the samples in this analysis. The principal component 1 score increases as one moves from composition D to composition A. This result supports the conclusion (obtained from the loading spectrum for principal component 1) that the first principal component is positively correlated to the hard block percentage. It is also noticed that the index (indicated by the middle digit of the sample name) within each cluster is positively correlated to the principal component 1 score. An increase in the index (excess isocyanate during the reaction) results in an increase in the fraction of aromatic CH groups (from the MDI functionality) and NH groups (from reaction of the isocyanate with other components) in the polymer. Although differences are expected in the NIR spectra of groups obtained from ideal (stoichiometric) reaction of isocyanate and from reaction of excess isocyanate, these differences are probably very small. As a result, the effects of hard block percentage and index are essentially the same in the NIR spectrum.

Variations in the densities of the samples are represented by variations in the principal component 2 scores. Note that the variation between the densities of the samples with composition B (indicated by the dispersion of sample labels with the

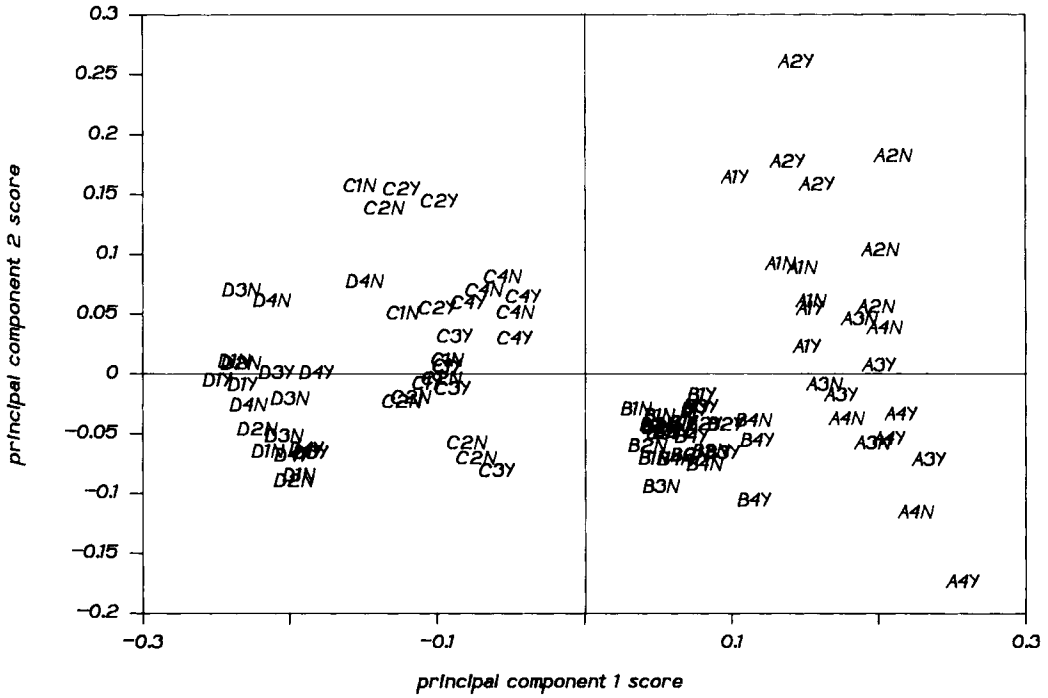

Figure 10 Plot of the second versus the first principal component scores, obtained from principal components analysis of the NIR spectra of the RIM polyurethanes in sample set **b**. Sample names are described in Table I.

first character *B* along the *y*-axis in Fig. 10) is much less than the variation between the densities of the samples with composition A. This result suggests that the densities of the samples with composition B were more accurately controlled during the RIM procedure than the densities of the samples with composition A.

The variation in the principal component 1 and principal component 2 scores of samples obtained from the same plaque reflects the nonhomogeneities of composition and density across single RIM plaques. For example, the principal component 1 scores for the three replicate samples obtained from plaque A3Y are significantly different. This result indicates the presence of significant compositional variations across plaque A3Y. The variation of the principal component 2 scores for the three replicate samples obtained from plaque A2N indicate a significant density variation across plaque A2N. The variation of composition and density across single plaques might be caused by incomplete mixing during the RIM procedure.

The third principal component loading spectrum is shown in Figure 9(C). Positive NH bands at 1502 and 2018 nm, a positive aromatic CH band at 1678 nm, and a positive MDI methylene band at 1762 nm indicate positive correlations to NH content and hard block percentage. The negative isocyanate band at 1882 nm indicates a negative correlation of this principal component with the amount of unreacted isocyanate groups in the polymer.

The 2-dimensional scores plot for principal components 1 and 3 is shown in Figure 11. It should be noted that samples from plaques C1Y and C1N each have exceptionally low values of the principal component 3 score, which indicates that these samples have exceptionally high concentrations of unreacted isocyanate groups. Visual inspection of these plaques reveals the presence of many defects, which were probably the result of incomplete mixing of the reactants during the RIM procedure. If incomplete mixing did occur during the preparation of these plaques, a significant amount of unreacted isocyanate groups is expected to be present in the samples obtained from these plaques. The higher principal component 3 scores for the post-cured samples (C1Y) relative to the non-post-cured samples (C1N) indicate that post-curing caused reaction of some of the isocyanate groups that were present in the original plaque. The positive correlation of the third principal component to NH content is observed because the reaction of isocyanate groups most commonly results in the formation of urethane NH groups.

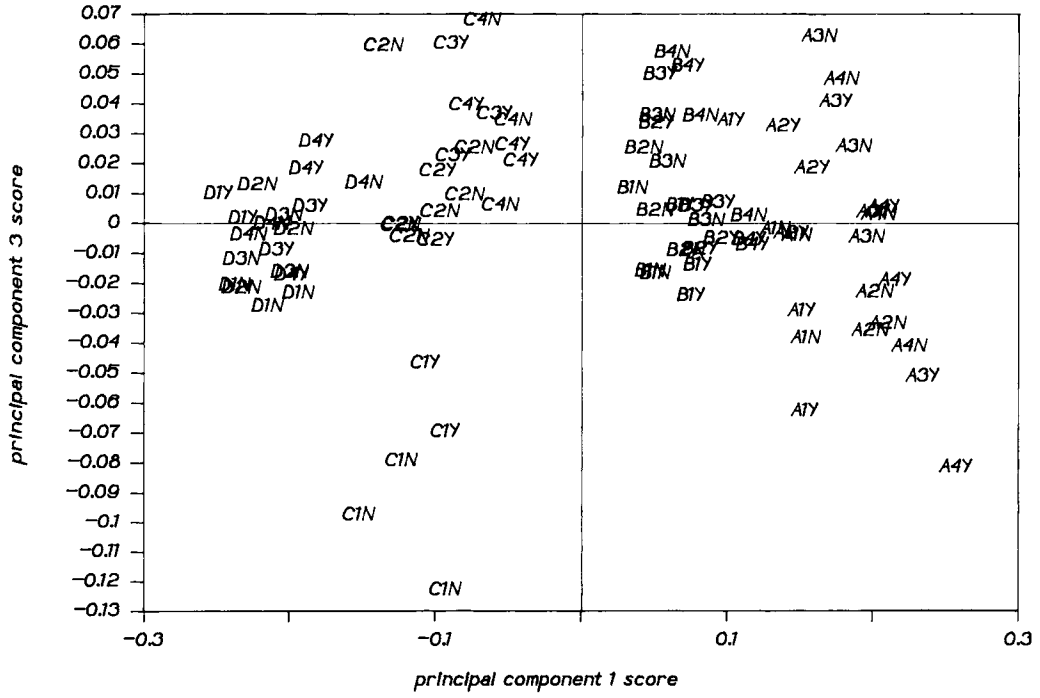

Figure 11 Plot of the third versus the first principal component scores, obtained from principal components analysis of the NIR spectra of the RIM polyurethanes in sample set **b**.

PLS Calibrations of Spectra to Physical Properties

Sample Set a

The results of PLS calibrations of NIR spectra to flex modulus and heat sag for samples in set **a** are shown in Table II. Cross-validation results indicate that three factors are required for all calibrations. NIR prediction errors are 4.0% relative for flex modulus at 23°C, and slightly higher for flex moduli at 38°C (5.9%) and 70°C (5.4%). These prediction errors are comparable to the estimated repeatability in the physical flex modulus measurement (7.96%). However, the relative NIR prediction error for heat sag (11.3%) is substantially higher than the estimated error in the reference method (2.26%). The lowest relative error of prediction is obtained for prediction of flex modulus at 23°C, because this property and the NIR spectra of the samples are measured at the same temperature. Prediction errors for flex moduli at 38 and 70°C and for heat sag are higher, because these properties depend on the state of the polymer at temperatures other than the temperature of NIR sampling. For prediction of the flex moduli at 38 and 70°C, it would be more appropriate to use the NIR spectra of the samples measured at 38 and 70°C. In addition, improved heat sag predictions might be obtained if the spectra of the polymers at 120°C are used. Unfortunately, these approaches might not be feasible for rapid process analysis.

The first PLS loading spectrum for the calibration to flex modulus at 23°C is shown in Figure 12. Positive aromatic CH peaks at 1140, 1648, and 2156 nm, a positive NH peak at 1500 nm, and negative aliphatic CH peaks at 1228 and 1736 nm are observed. This result indicates that the modulus at 23°C is positively correlated to hard block percentage.

The positive band at 1984 nm (hydrogen-bonded urethane carbonyl group), the negative band at 1920 nm (free urethane carbonyl group), and the positive band at 2028 nm (free urea carbonyl group) might indicate decreasing phase separation of the hard and soft blocks in the polymers.[24] If this is the case, this result indicates that the flex modulus increases with decreasing phase separation. However, it is expected that phase separation, which increases the effective crosslinking of the polymer chains, increases the modulus of a block copolymer. In light of this discrepancy, the observed inverse relationship between flex modulus and phase separation might actually reflect the experimental design, in which an inverse relationship exists between hard block percentage and phase separation, for the samples used in this analysis. If this is the case, the individual effects of hard block percentage and phase separation on the flex modulus cannot be assigned, because the two properties are correlated. However, we observe that the flex modulus is positively correlated to hard block percentage, because the hard block percentage

Table II Results of PLS Calibrations of NIR Spectra to Physical Properties of RIM Polyurethanes

	Calibration			Prediction			
Property (units)	SEE	Range	Relative Error (%)	SEP	Range	Relative Error (%)	Repeatability of Reference Method (%)[a]
			Sample Set **a**				
Flex modulus, 23°C ($\times 10^{-7}$ N/m^2)	1.26	23.7–55.0	4.0	1.23	24.6–54.2	4.0	7.96
Flex modulus, 38°C ($\times 10^{-7}$ N/m^2)	1.68	19.0–45.3	6.4	1.36	19.4–42.6	5.9	7.96
Flex modulus, 70°C ($\times 10^{-7}$ N/m^2)	0.83	14.2–31.0	5.0	0.79	14.4–29.0	5.4	7.96
Heat sag (cm)	0.32	0.71–3.81	10.3	0.28	0.97–3.48	11.3	2.26
			Sample Set **b**				
Flex modulus, 23°C ($\times 10^{-7}$ N/m^2)	3.2	4.0–47.5	7.5	3.7	4.1–46.2	8.9	7.96
Heat sag (cm)	0.36	1.19–4.24	12.0	0.43	1.32–3.66	18.6	2.26

[a] Repeatability values expressed as percentage of the mean; these values are obtained from within-lab replicate measurement of several samples (see Ref. 35 for flex modulus, Ref. 36 for heat sag).

has a stronger effect on the flex modulus (and on the NIR spectra) than the phase separation.

The effect of density [indicated by the spectral pattern shown in Fig. 6(A)] on the flex modulus is difficult to detect in the PLS loading spectrum for flex modulus (Fig. 12). As a result, the effect of density on the flex modulus cannot be determined from these results. It should be noted that the corresponding PLS loading spectra for the flex modulus at 38 and 70°C are very similar to the loading spectrum for flex modulus at 23°C (Fig. 12).

The first PLS loading spectrum for the calibration to heat sag is shown in Figure 13. This plot is almost identical to the first PLS loading spectrum for the flex modulus calibration (Fig. 12). As a result, it can be tentatively concluded that heat sag increases with increasing hard block percentage for the samples in set **a**.

The positive correlation of heat sag to hard block percentage for the samples in set **a** can be explained by a "compression set" mechanism. A compression set measurement, which is similar to a heat sag measurement, involves the compression of a sample for approximately 24 h at an elevated temperature, and removal of the load to allow the sample to recover.[3] During the hot compression, breaking and reforming of hydrogen bonds in the hard segment blocks can occur. The new hydrogen bonds are in equilibrium with the compressed state, and serve to retain the compressed state against recovery of the polymer. At the temperature of the heat sag measurement (120°C, kT = 0.78 kcal/mol) substantial breaking of the N—H..O=C hydrogen bonds in the hard blocks (with a hydrogen bond strength of approximately 3.5 kcal/mol[51]) is possible. If a hydrogen bond breaking and reforming mechanism is an accurate model for heat sag in these polymers, it is expected that this property is proportional to the number of possible hydrogen bond pairs (or the hard block percentage).

Sample Set b

The results of PLS calibrations for flex modulus at 23°C and heat sag of the sample set **b** samples are shown in Table II. Three PLS factors were used for both calibrations. As in the set **a** analyses, the relative error of prediction for flex modulus at 23°C (8.9%) is comparable to the estimated precision of the reference method (7.96%),[41] and the relative error of prediction for heat sag (18.6%) is substantially higher than the estimated precision of the reference method (2.26%).[42] As mentioned earlier, the error for the heat sag calibration is higher because the heat sag depends on the state of the polymer at an elevated temperature, which is difficult to deter-

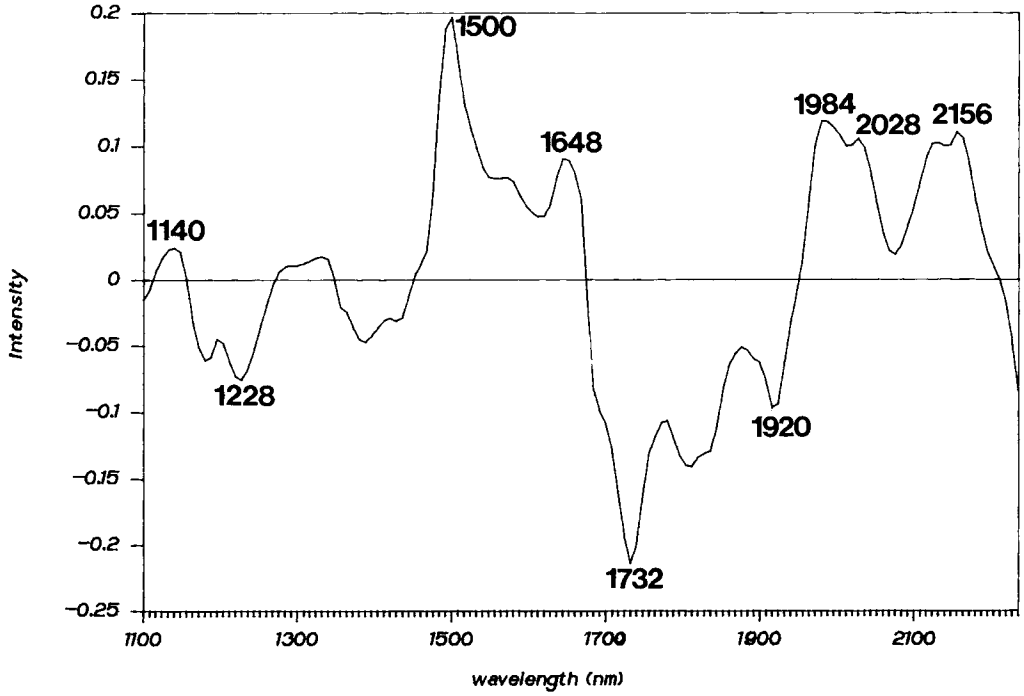

Figure 12 First PLS loading spectrum for the calibration to flex modulus at 23°C, obtained from the samples in set **a**.

mine from the spectrum of the polymer at room temperature.

Table II also indicates that the calibration and prediction errors for flex modulus at 23°C of the sample set **b** samples are much higher than the corresponding errors for flex modulus at 23°C of the sample set **a** samples. The source of this discrepancy is indicated by observation of the PLS calibration curves for the calibration to flex modulus at 23°C derived from sample set **a** (Fig. 14) and sample set **b** (Fig. 15). The major difference between these two calibration curves is the presence of large deviations in the sample set **b** calibration curve for samples with very high or very low flex moduli. This result might indicate systematic errors in the reference flex modulus measurement for samples with very high or very low flex moduli, or a nonlinear relationship between NIR spectral absorbances and flex modulus for the samples in set **b**. The lack of this effect for the high flex modulus samples in the sample set **a** calibration curve (Fig. 14) indicates that systematic errors in the reference measurement for high flex modulus samples are not present. As a result, the apparent curvature in the sample set **b** calibration curve is probably caused by a nonlinear relationship between NIR absorbances and flex modulus. The lack of such curvature in the sample set **a** calibration curve might be caused by the fact that the samples in set **a** are in a "linear" region, where the relationship between NIR absorbances and flex modulus is approximately linear.

The first PLS loading spectrum for the calibration to flex modulus (Fig. 16) has positive aromatic CH bands (1142 and 1645 nm), positive NH bands (1494 and 1998 nm) and negative aliphatic CH bands (1230 and 1734 nm). This result indicates that the flex modulus is positively correlated to the hard block percentage, which is concurrent with results obtained from set **a**. The effect of phase separation on the flex modulus is difficult to determine from the first PLS loading spectrum. The negative band at 1922 nm might correspond to a decrease in the amount of free urethane carbonyl groups or to a decrease of the amount of moisture in the polymer.[24]

The density effect [shown in Figs. 6(A) and 9(B)] is observed in the first PLS loading spectrum (Fig. 16). Although the 1142 nm aromatic CH band is positive, the 2148 nm aromatic CH band is negative in the PLS loading spectrum (Fig. 16). This result indicates that the flex modulus is correlated with an enhancement of shorter-wavelength diffuse reflectance intensities relative to longer-wavelength intensities, which (according to an argument in a previous section) is correlated to an increase in the density. Therefore, our data indicate that the flex modulus is positively correlated to the density.

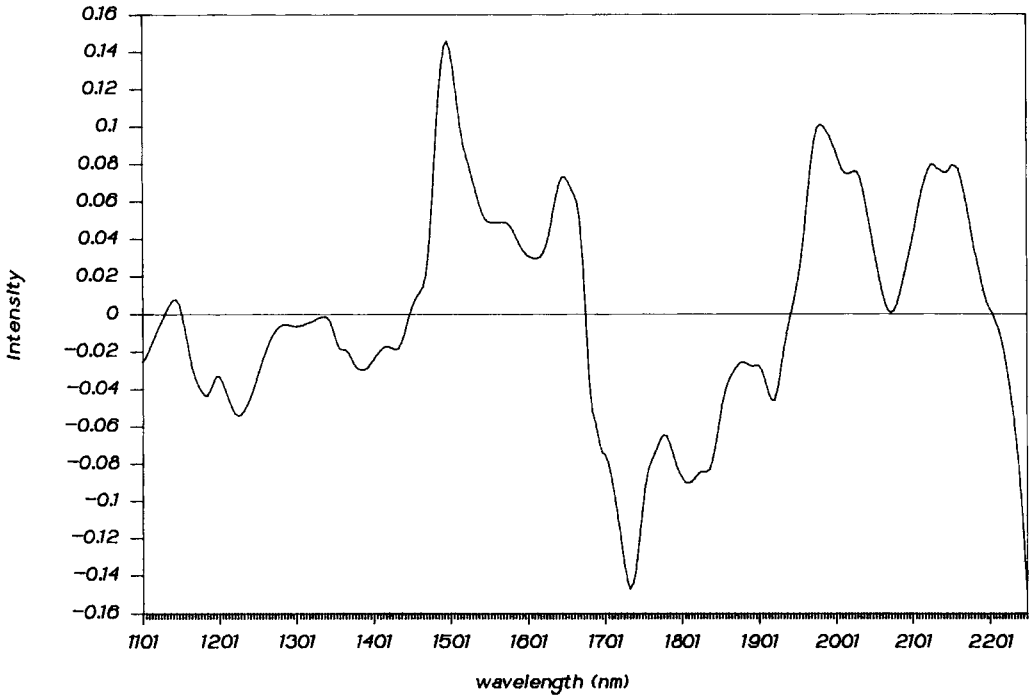

Figure 13 First PLS loading spectrum for the calibration to heat sag, obtained from the samples in set **a**.

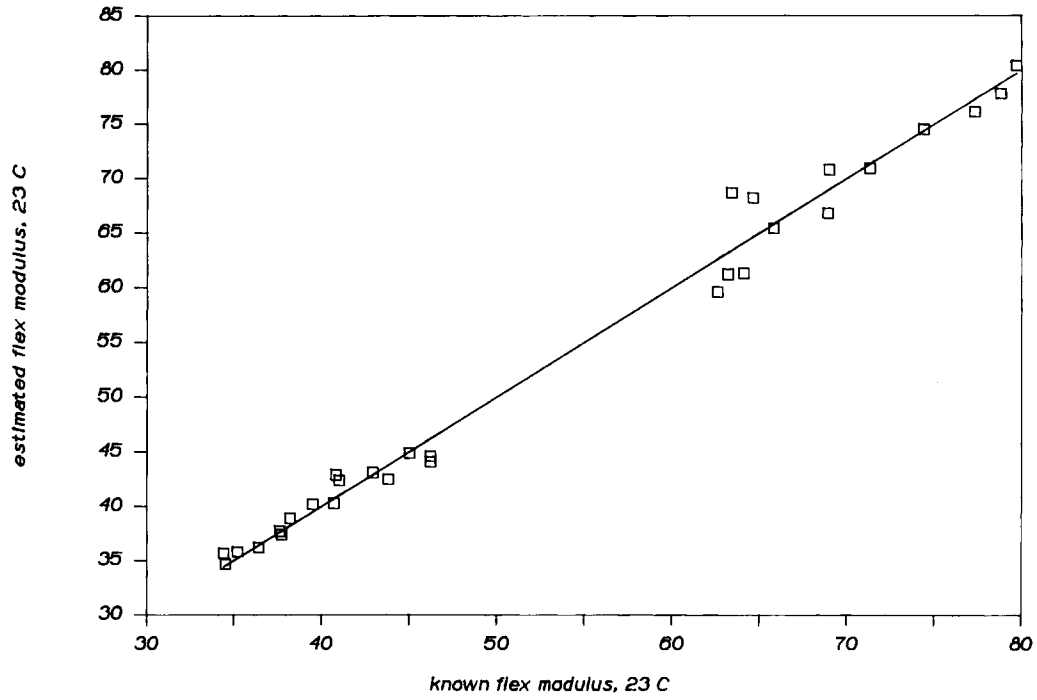

Figure 14 Calibration curve for the PLS calibration of near-infrared spectra to flex modulus at 23°C, derived from the polyurethane samples in set **a**.

The first PLS loading spectrum for the calibration to heat sag is shown in Figure 17. The positive band at 1734 nm and the negative bands at 1494 and 1654 nm indicate an inverse dependence of heat sag on hard block percentage. In addition, the positive long-wavelength aromatic CH peak at 2158 nm and the negative short-wavelength aromatic CH peak at 1142 nm indicate an inverse dependence of heat sag

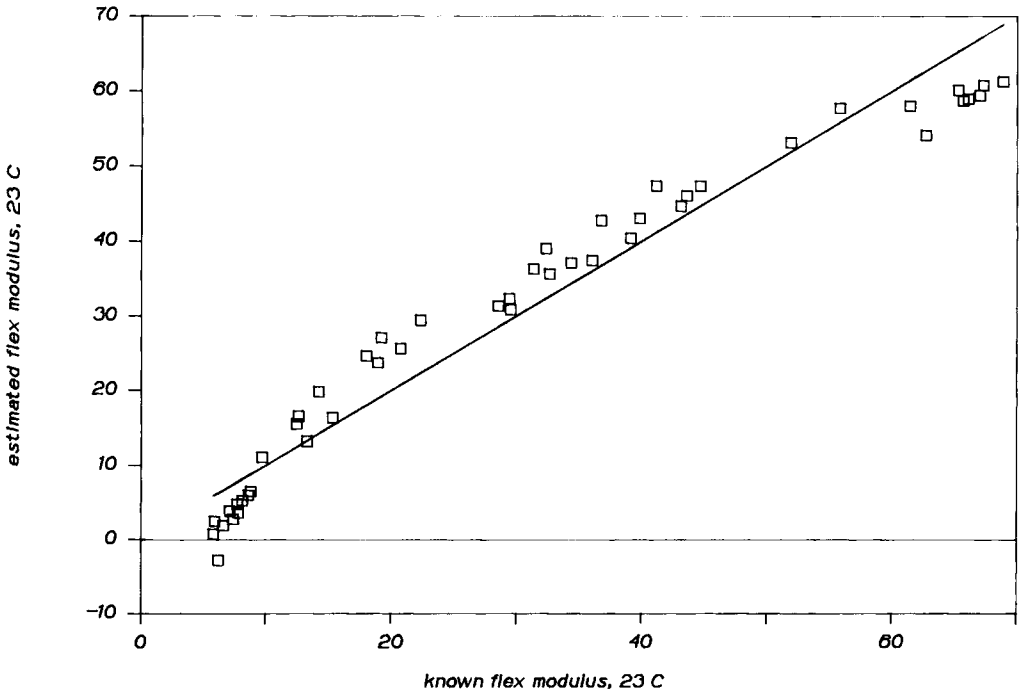

Figure 15 Calibration curve for the PLS calibration of near-infrared spectra to flex modulus at 23°C, derived from the polyurethane samples in set **b**.

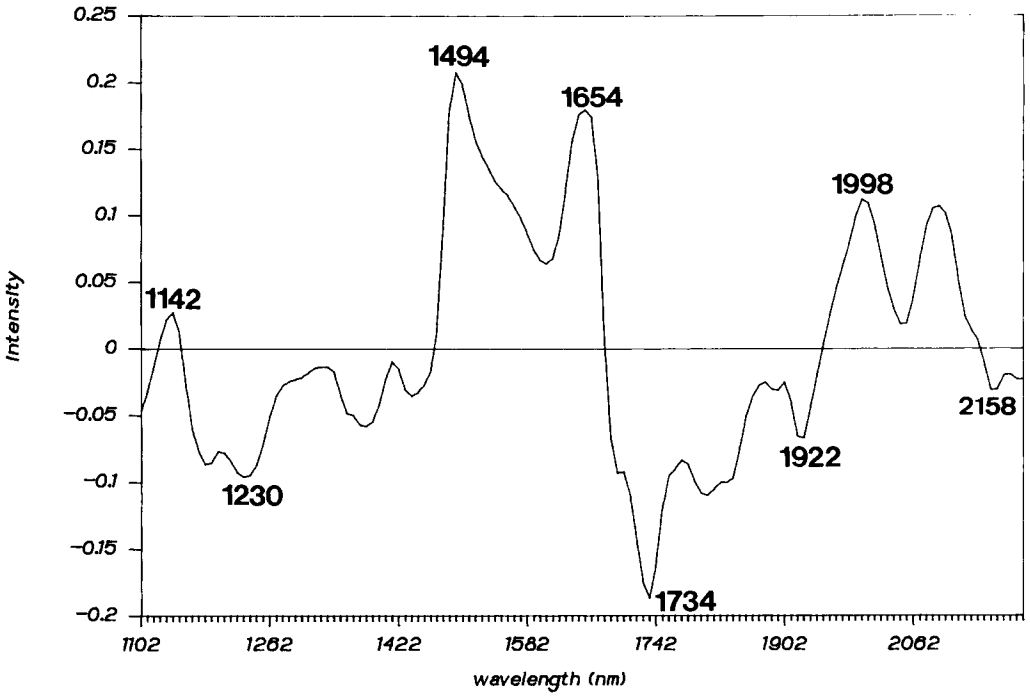

Figure 16 First PLS loading spectrum for the calibration to flex modulus at 23°C, derived from the samples in set **b**.

on density. The negative peak at 1878 nm indicates an inverse dependence on the amount of unreacted isocyanate groups in the polymers.

It should be noted that the dependence of heat sag on the hard block percentage is exactly the opposite of the result obtained for the samples in set **a** (Fig. 13). This discrepancy indicates that a general relationship between hard block percentage and heat

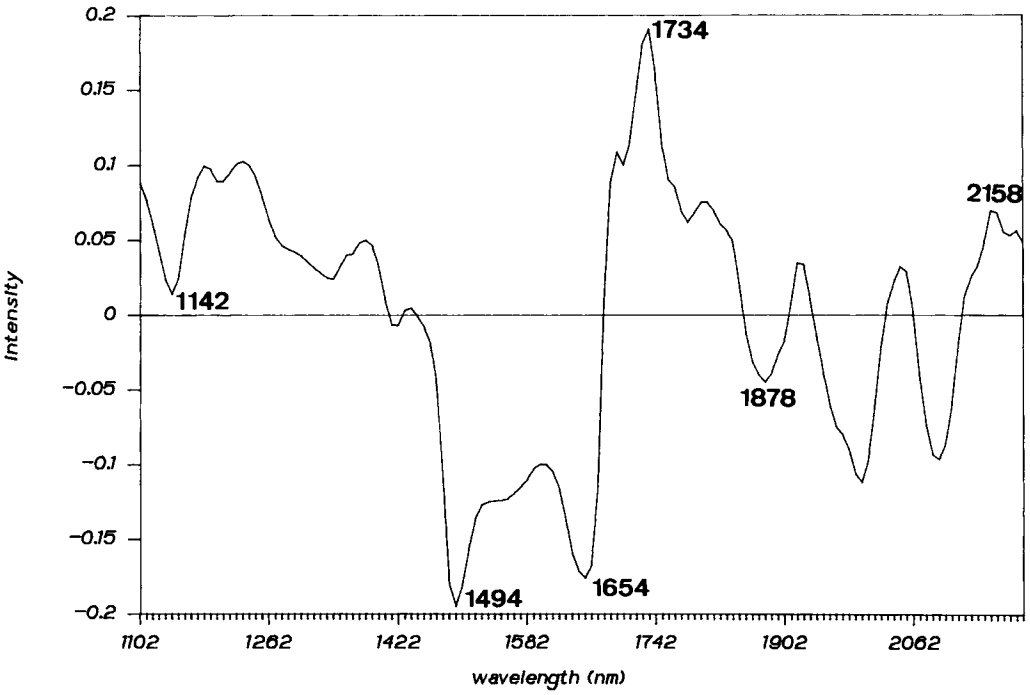

Figure 17 First PLS loading spectrum for the calibration to heat sag, derived from the samples in set **b**.

sag does not exist, or that heat sag depends greatly on the specific polymer system studied. It is possible that the heat sag is greatly influenced by other properties, such as phase separation and morphology of the hard and soft blocks, which are in turn influenced by the specific chemistry of the polymer system and the RIM processing procedure. Unfortunately, it is difficult to determine specific effects of these properties on the heat sag from our results, because the effects of these properties in the NIR spectra are quite weak and the stronger effects of hard block percentage and density dominate the PLS loading spectra. Despite these difficulties, our calibration and prediction results indicate that NIR spectroscopy contains sufficient information to predict the heat sag of RIM polyurethanes.

Moisture Content

Figure 18 shows the spectra of sample A2E (in sample set **a**) before drying (a), after drying at 120°C for 90 min (b), and after 20 additional hours at room temperature in the open atmosphere (c). The heating procedure (a to b) caused a decrease in the absorbance of the first overtone OH stretching band at 1430 nm and the combination OH stretching and bending band at 1922 nm. These bands have been previously assigned to water absorbances.[19] Subsequent exposure of the sample to the atmosphere (b to c) allowed the dried polymer to absorb moisture from the air, which caused an increase in the intensities of these moisture bands.

The absorbance at 1572 nm behaves in the same way as the moisture bands. This absorbance is in the region of first overtone stretching bands of NH groups that are hydrogen bonded. The behavior of this absorbance with respect to moisture content suggests that it is a band for an NH–water hydrogen-bonded complex in the polymer.

Figure 18 shows that the changes in the moisture bands at 1430 and 1922 nm and the NH–water complex band at 1572 nm are clearly greater than the spectral noise level. As a result, these bands can be used to determine moisture content in the polymer. Figure 19 shows the absorbance of these three bands versus the total mass of polymer weighed after each spectrum was taken. It is assumed that the only mass changes in the polymer during this experiment were from moisture loss or gain. The estimated error of the mass measurements is ±0.0001 g. The correlations between each of the three absorbances and moisture content (correlation coefficients = 0.998 for 1430 nm, 0.992 for 1572 nm, and 0.986 for 1922 nm) are very high.

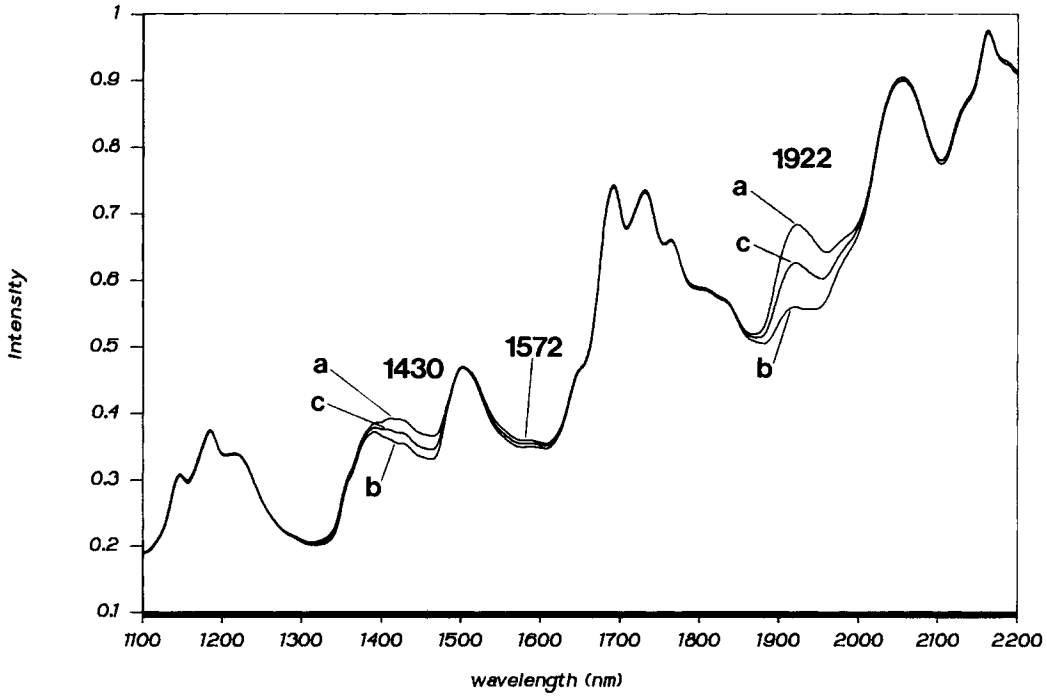

Figure 18 Near-infrared diffuse reflectance spectrum of RIM sample A2E (in sample set **a**) as received (a), after 1.5 h drying at 120°C (b), and after 20 additional hours exposed to the atmosphere at room temperature (c).

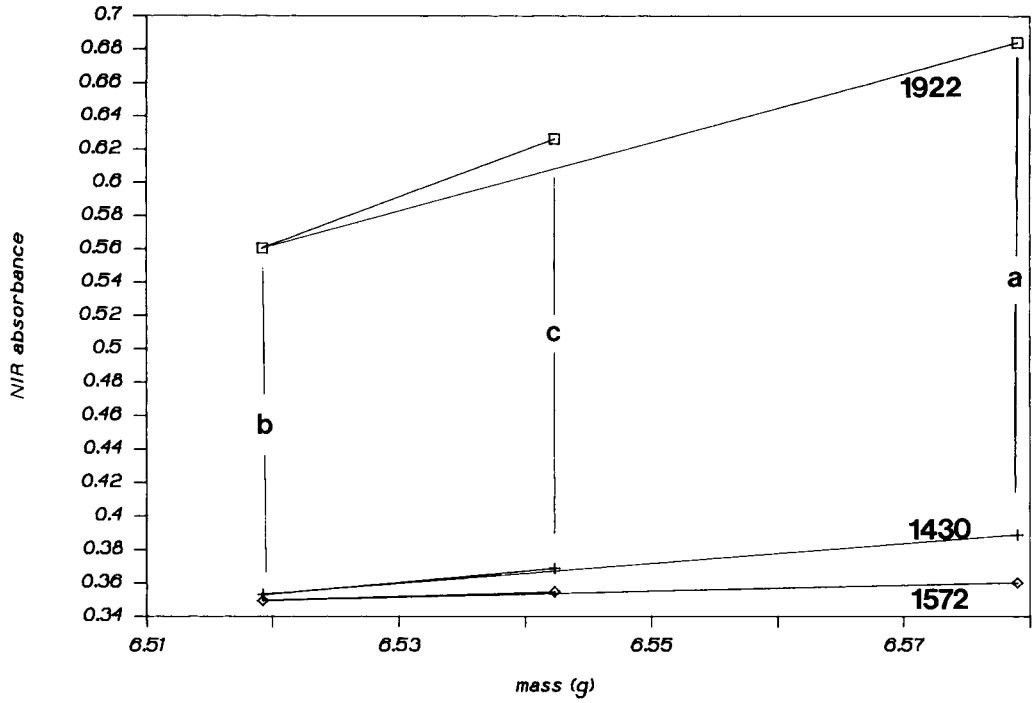

Figure 19 Spectral intensities at three different near-infrared wavelengths versus the mass of the sample during the moisture study.

The correlation to moisture is lowest for the 1922 nm absorbance. This result is probably caused by interference of the moisture absorbance at this wavelength with the free urethane carbonyl absorbance at 1916 nm[24] [Fig. 4(B)]. Phase separation, which (for the diamine-extended polymers used in sample set **a**) is probably accompanied by an increase in the intensity of the free urethane carbonyl band,[24] might occur during the drying procedure. If this is the case, the decrease in water absorbance during the drying step (a to b, in Fig. 19) is partially offset by the increase in the absorbance of the overlapping free urethane carbonyl band. The moisture regaining step (b to c) involves a larger slope in the absorbance versus mass curve, because no offsetting effect of phase separation occurs.

CONCLUSION

Near infrared spectroscopy can provide rapid and accurate predictions of flex modulus and heat sag in RIM polyurethanes. Accurate determinations are possible because NIR spectroscopy can detect changes in composition, density, and phase separation, which affect physical properties. It was found that NIR spectra of RIM polyurethanes at room temperature can be used to predict physical properties of the materials at elevated temperatures. Moisture in the polymer is correlated to the absorbance of OH overtone and combination bands from water, and by an NH stretching overtone band from an NH–water hydrogen-bonded complex.

This work was supported by a grant from ICI Polyurethanes. Specific acknowledgements go to Dr. W. W. Brand and A. Hurst, for coordinating the research, Dr. R. E. Camargo, Dr. J. Yavorsky, K. Woolson, and J. Boone for consulting and guidance with reaction-injection-molding, and Al Flint and Stewart Smith for information regarding physical tests. Editing comments provided by Dr. R. E. Camargo were very helpful. Flex modulus and heat sag measurements, performed by Donna Boody, were essential for this work.

REFERENCES

1. C. W. Macosko, *RIM, Fundamentals of Reaction Injection Molding,* Hanser, Munich, 1989.
2. G. Woods, *Mod. Plast.*, **64**(10A), 122 (1987).
3. J. H. Saunders and K. C. Frisch, *Polyurethanes, Chemistry and Technology, Part I: Chemistry,* Wiley-Interscience, New York, 1962, pp. 329–337.
4. Z. S. Chen, W. P. Yang, and C. W. Macosko, *Rubber Chem. Technol.*, **61**, 86 (1988).
5. J. Blackwell, J. R. Quay, and R. B. Turner, *Polym. Eng. Sci.*, **23**, 816 (1983).

6. R. E. Camargo, C. W. Macosko, M. V. Tirrell, and S. T. Wellinghoff, *Polymer*, **26**, 1145 (1985).
7. R. E. Camargo, C. W. Macosko, M. V. Tirrell, and S. T. Wellinghoff, *Polym. Eng. Sci.*, **22**, 719 (1982).
8. W. P. Yang and C. W. Macosko, *Makromol. Chem. Macromol. Symp.*, **25**, 23 (1989).
9. ASTM Method C518-85, "1988 Annual Book of ASTM Standards," *ASTM, Philadelphia, 1988.* **4-06**, p. 151.
10. T. Provder, *J. Coatings Technol.*, **61**, 33 (1989).
11. P. C. Hiemenz, *Polymer Chemistry*, Dekker, New York, 1984.
12. R. E. Camargo, C. W. Macosko, M. V. Tirrell, and S. T. Wellinghoff, *Polym. Commun.*, **24**, 314 (1983).
13. M. A. Harthcock, *Polymer*, **30**, 1234 (1989).
14. H. V. Drushel, *CRC Crit. Rev. Anal. Chem.*, **1**, 161 (1970).
15. H. S. Lee and S. L. Hsu, *Macromolecules*, **22**, 1100 (1989).
16. S. K. Pollack, D. Y. Shen, S. L. Hsu, Q. Wang, and H. D. Stidham, *Macromolecules*, **22**, 551 (1989).
17. J. Blackwell and C. P. Lee, *J. Polym. Sci. Polym. Phys. Ed.*, **22**, 759 (1984).
18. L. G. Weyer, *Appl. Spectrosc. Rev.*, **21**, 1 (1985).
19. I. Murray and P. C. Williams, in *Near-Infrared Technology in the Agricultural and Food Industries*, American Association of Cereal Chemists, St. Paul, MN, 1987, Chap. 2.
20. E. Stark, K. Luchter, and M. Margoshes, *Appl. Spectrosc. Rev.*, **22**(4), 335 (1986).
21. C. E. Miller, *Appl. Spectrosc.*, **43**(8), 1435 (1989).
22. C. E. Miller and B. E. Eichinger, *Appl. Spectrosc.*, **44**(3), 496 (1990).
23. C. E. Miller, P. G. Edelman, and B. D. Ratner, *Appl. Spectrosc.*, **44**(4), 576 (1990).
24. C. E. Miller, P. G. Edelman, B. D. Ratner, and B. E. Eichinger, *Appl. Spectrosc.*, **44**(4), 581 (1990).
25. C. E. Miller, B. E. Eichinger, T. W. Gurley, and J. G. Hermiller, *Anal. Chem.*, **62**, 1778 (1990).
26. H. Martens, T. Naes, in *Near-Infrared Technology in the Agricultural and Food Industries*, American Association of Cereal Chemists, St. Paul, MN, 1987, Chap. 4.
27. I. T. Jolliffe, *Principal Component Analysis*, Springer-Verlag, New York, 1986.
28. M. A. Sharaf, D. L. Illman, and B. R. Kowalski, *Chemometrics*, Wiley, New York, 1986.
29. K. Beebe and B. R. Kowalski, *Anal. Chem.*, **39**, 1007A (1987).
30. P. Geladi and B. R. Kowalski, *Anal. Chim. Acta*, **185**, 1 (1986).
31. D. M. Haaland and E. V. Thomas, *Anal. Chem.*, **60**, 1193 (1988).
32. H. L. C. Meuzelaar and T. L. Isenhour, *Computer-Enhanced Analytical Spectroscopy*, Plenum, New York, 1987.
33. W. Windig, J. Haverkamp, and P. G. Kistemaker, *Anal. Chem.*, **55**, 81 (1983).
34. D. van de Meent, J. W. de Leeuw, P. A. Schenck, and J. Haverkamp, *J. Anal. Appl. Pyrol.*, **4**, 133 (1982).
35. W. Windig, G. S. de Hoog, and J. Haverkamp, *J. Anal. Appl. Pyrol.*, **3**, 213, (1982).
36. R. Tsao and K. J. Voorhees, *Anal. Chem.*, **56**, 368 (1984).
37. K. H. Voorhees and R. Tsao, *Anal. Chem.*, **57**, 1630 (1985).
38. J. L. Ilari, H. Martens, and T. Isaksson, *Appl. Spectrosc.*, **42**, 722 (1988).
39. P. Geladi, D. MacDougall, and H. Martens, *Appl. Spectrosc.*, **39**, 491 (1985).
40. P. Yeo and D. E. Honigs, *Appl. Spectrosc.*, **42**, 1128 (1988).
41. ASTM Method D790-86, *1989 Annual Book of ASTM Standards*, ASTM, Philadelphia, 1989, 08.01, p. 280.
42. ASTM Method D3769-85, *1989 Annual Book of ASTM Standards, ASTM*, Philadelphia, 1989, 09.02, p. 370.
43. D. Veltkamp, *PCA Modeling Program, Version 1.0 (IBM)*, Center for Process Analytical Chemistry, BG-10, Seattle, WA 98195, 1989.
44. D. Veltkamp and B. R. Kowalski, *PLS-2 Block Modeling, Version 1.9 (IBM)*, Center for Process Analytical Chemistry, BG-10, Seattle, WA 98195, 1986.
45. L. Born, H. Hespe, J. Crone, and K. H. Wolf, *Colloid Polym. Sci.*, **260**, 819 (1982).
46. W. Willkomm, Ph.D. thesis, University of Minnesota, 1990.
47. G. S. Birth and H. G. Hecht, in *Near-Infrared Technology in the Agricultural and Food Industries*, American Association of Cereal Chemists, St. Paul, MN, 1987, Chap. 1.
48. G. Kortum, *Reflectance Spectroscopy*, Springer-Verlag, New York, 1969, Chap. 2, p. 23.
49. A. M. C. Davies and C. E. Miller, *Appl. Spectrosc.*, **42**, 703 (1988).
50. G. Pimental and A. L. McClellan, *The Hydrogen Bond*, Freeman, San Francisco, 1960.
51. P. Schuster, G. Zundel, and C. Sandorfy, *The Hydrogen Bond, II. Structure and Spectroscopy*, North-Holland, New York, 1976.
52. C. E. Miller and D. E. Honigs, *Spectroscopy*, **4**, 44 (1989).

Received March 26, 1990
Accepted August 2, 1990